NEOPLASMA accepted, ahead of print manuscript
Cite article as https://doi.org/10.4149/neo_2026_260223N45

Running title: circ_0005882 suppresses NPC proliferation

YTHDF2-regulated hsa_circ_0005882 functions as a sponge for miR-654-3p to suppress nasopharyngeal carcinoma proliferation

Xu Wang[1,2,#], Aiyu Ma[1,2,#], Lu Lu[1], Qiuyu Zhao[1], Yuzhong Yang[1], Xuan Meng[1], Yiping Sun[1], Shuming Wang[1], Zhiyi Chen[1], Yan Zhang[1], Jinhua Zheng[1,2], Xiang Zheng[1,2,*]

[1]Department of Pathology, The First Affiliated Hospital of Guilin Medical University, Guilin, Guangxi, China; [2]Guangxi Key Laboratory of Multimodal Biomarkers and Precision Diagnosis, Guilin Medical University, Guilin, Guangxi, China

*Correspondence: xiangzheng12@sina.com

[#]Contributed equally to this work.

Received February 23, 2026 / Accepted June 25, 2026

Circular RNAs (circRNAs) are a subclass of non-coding RNAs, playing an important regulatory role in tumor progression. Accumulating evidence has revealed that circRNAs can be regulated by m6A machinery, influencing their expression and biological functions. However, the functions and mechanisms of m6A-mediated circRNAs in nasopharyngeal carcinoma (NPC) remain to be elucidated. In this study, the sequence of hsa_circ_0005882 (circ_0005882) was determined by Sanger sequencing, and its localization in both the cytoplasm and nucleus was confirmed by fluorescence in situ hybridization. Furthermore, m6A RNA immunoprecipitation followed by qPCR (MeRIP-qPCR) and the single-base elongation- and ligation-based qPCR amplification (SELECT) assays revealed that circ_0005882 may harbor m6A modifications. Overexpression of circ_0005882 significantly suppressed NPC cell proliferation. Mechanistically, the m6A reader YTHDF2 binds to circ_0005882 to promote its degradation, thereby reducing circ_0005882 stability. Additionally, circ_0005882 functions as a sponge for miR-654-3p, contributing to the inhibition of NPC proliferation. These findings collectively demonstrate that circ_0005882, which is negatively regulated by YTHDF2, functions as a tumor suppressor by sponging miR-654-3p to inhibit NPC cell proliferation, unveiling a novel regulatory model centered on the YTHDF2/circ_0005882/miR-654-3p axis in NPC pathogenesis.

Key words: circ_0005882; miR-654-3p; YTHDF2; m6A; nasopharyngeal carcinoma

Nasopharyngeal carcinoma (NPC) is a malignant tumor originating from the nasopharyngeal mucosal epithelium. Its incidence exhibits a significant geographical distribution disparity worldwide, with particularly high rates in Southern China and Southeast Asia [1, 2]. Due to its

insidious and nonspecific early presentation, NPC is often diagnosed late, missing the optimal period for intervention. Consequently, patients with advanced-stage NPC frequently experience treatment failure due to disease recurrence or distant metastasis [3]. Although advances have been made in treating NPC with radiotherapy, chemotherapy, and targeted therapy, the underlying molecular mechanisms of NPC remain incompletely understood. Further investigation into the pathogenesis of NPC is therefore necessary to identify novel therapeutic targets and enhance anti-tumor efficacy.

circRNAs, a subclass of non-coding RNAs, are characterized by their evolutionary conservation and notable structural stability. Distinct from conventional linear RNAs, circRNAs lack both 5′ cap and 3′ poly(A) tail and are characterized by their formation via back-splicing to form covalently closed circular structures via 5′-3′phosphodiester bonds [4]. This covalently closed circular structure protects circRNAs from exonuclease-mediated degradation, thereby conferring high stability [5, 6]. Current research has shown that circRNAs are closely associated with tumorigenesis, and aberrant circRNA expression has been observed in many types of cancer [7-11].

N6-methyladenosine (m6A) modification is the most prevalent internal modification in eukaryotic RNAs and dynamically regulates RNA metabolism through the coordinated actions of “writers”, “erasers”, and “readers” [12]. As a reversible and tightly controlled process, m6A plays a crucial role in regulating mRNA stability, splicing, and translation and is closely associated with tumorigenesis and progression [13-15]. YTHDF2, a canonical m6A reader protein, selectively recognizes m6A-modified RNAs and regulates their stability, which is a key mechanism for modulating gene expression programs in cancer [16-18]. Increasing studies have demonstrated that aberrant YTHDF2 expression contributes to the growth, malignant progression and tumor immune evasion of multiple cancer types [17, 19, 20]. In recent years, accumulating evidence has revealed that some circRNAs are also regulated by m6A modification, which influences their stability and biological functions [21, 22]. However, the functional significance of m6A-modified circRNAs and their regulation by m6A machinery in NPC remains to be elucidated.

In this study, we identified that *circ_0005882*, derived from exons 9 to 14 of the serine/threonine kinase 39 (*STK39)* gene via back- splicing, functions as a tumor suppressor to inhibiting NPC cells proliferation by sponging *miR-654-3p*. Further analyses indicated YTHDF2 decreased *circ_0005882* stability in an m6A-dependent manner. Our work uncovers a novel

YTHDF2/*circ_0005882*/*miR-654-3p* axis and elucidates its role in epitranscriptomic dysregulation during NPC tumorigenesis.

Materials and methods

Cell cultures and reagents. NP69, an immortalized normal nasopharyngeal epithelial cell line, was purchased from Otwo Biotech (China). NPC cell lines 5-8F and HNE1 were kindly provided by Central South University. Cells were cultured in Dulbecco's modified Eagle's medium (Gibco, USA) supplemented with 10% fetal bovine serum (#S711-050S, Lonsera, China), penicillin and streptomycin (100 U/ml, #P1400, Solarbio, China) in a humidified incubator at 37 °C with 5% CO_2. YTHDF2 overexpression vector and control vector were purchased from Hunan Fenghui Biotechnology Company (China). siRNAs were purchased from RIBOBIO (China). *miR-654-3p* mimics and inhibitors were purchased from Sangon Biotech (China). *Circ_0005882* overexpression vector (pLC5-circ_0005882), si-circ_0005882 were purchased from GENSEED (China). The cells were transfected with RNAs and/or plasmids using Lipofectamine 3000 (#L300015, Invitrogen, USA). Sequences are listed in Supplementary Table S1.

Nuclear and cytoplasmic fractionation. The nuclear and cytoplasmic fractionation was conducted using the PARIS™ Kit (#AM1921, Thermo Fisher Scientific, USA) following the manufacturer's instruction. Subsequently, the levels of *circ_0005882* distributed in the cytoplasmic and nuclear compartments of NPC cells were quantified by RT-qPCR. *GAPDH* and *U6* were used as the internal references for cytoplasmic and nuclear localized RNA, respectively.

Reverse transcription quantitative polymerase chain reaction (RT-qPCR). Total RNA was extracted using TRIzol reagent (#9108, Takara, Japan). For mRNA and circRNA detection, reverse transcription was performed using the RevertAid™ First Strand cDNA Synthesis Kit with DNase I (#K16225, Thermo Fisher Scientific, USA). For miRNA detection, reverse transcription was carried out by the miRNA 1st Strand cDNA Synthesis Kit (#MR201-01, Vazyme, China). qPCR was performed by Applied Biosystems system (Thermo Fisher Scientific, USA) using SYBR Green Master Mix (#EG20117M, Yugong Biotech, China). The relative expression levels were calculated by the cycle threshold (Ct) method. *GAPDH* and *U6* were used to normalize the expression of mRNA and miRNA respectively. The primers used for qPCR are listed in Supplementary Table S2.

Lentiviral transduction of target cells. For lentiviral production, 293T cells were seeded into 10

cm dish (2×10^6/ well) and were co-transfected with 8 μg pLC5-circ_0005882 vectors and components of packaging vectors: 5.28 μg pLP1 and 4 μg pLP2 packaging vector and 2.8 μg VSVG envelope vector, using Lipo293™ transfection reagent (#C0521, Beyotime Biotechnology), according to the manufacturer's protocol. The lentivirus-containing supernatant was harvested at 48 h and 72 h post-transfection, filtered and then used to transduce the target 5-8F or HNE1 cells at a multiplicity of infection (MOI) of 10. After 48 h transfection, 5 μg/ml puromycin (#P8230, Solarbio, China) was added in culture medium to screen stable transfected cells for 7 days. Surviving cells were selected for subsequent culture after continuous puromycin administration. All sequences used were verified by DNA sequencing, and the overexpression efficiency of *circ_0005882* was confirmed by RT-qPCR.

CCK-8 assay. A total of 1,000 cells in a volume of 100 μl/well were cultured in five replicate wells in a 96-well plate in medium containing 10% FBS. Then, 10 μl CCK-8 reagent (#GK10001, GLPBIO, China) was added to 90 μl DMEM/RPMI 1640 to generate a working solution, of which 100 μl was added per well and incubated for 2 h. Absorbance measurements were taken at various time points, including 0 h, 24 h, 48 h, 72 h and 96 h.

EdU assay. Cells were seeded into 96-well plates and cultured overnight, followed by the addition of an equal volume of 2× EdU working solution (20 μM). After incubation at 37 °C, with 5% CO_2 for 2 h, the cells were fixed with 4% paraformaldehyde overnight and incubated with 0.3% Triton-X-100 in PBS for 15 min. The nuclei were stained with Hoechst dye 33,342 (BeyoClick™EdU-555 Kit, #C0075S, Beyotime Biotechnology). Images of five randomly selected areas of each group were taken with a fluorescence microscope (Thermofisher Scientific).

Fluorescence *in situ* hybridization (FISH). A cy3-labeled probe crossed the splice junction sequence against *circ_0005882* was designed and synthesized by GenePharma. Cells were inoculated into 24-well plate and cultured in 10% FBS, the plate was fixed by incubation with 4% paraformaldehyde for 15 min at room temperature, then washed with PBS. The fixed cells were incubated with 0.1% buffer A for 15 min at room temperature. Subsequently, cells were incubated with pre-hybridization buffer for 30 min at 37 °C prior to the addition of probes in hybridization buffer for 73 °C 5 min and 37 °C overnight. Next, the cover liquid was removed, and the cells were washed with 0.1% Buffer F, 2× buffer C and 1× buffer C for 3 × 5 min at room temperature. The nuclei were stained with DAPI for 20 min at room temperature. The cell localization was detected

by laser scanning confocal image system. The pre-hybridization buffer and hybridization buffer were obtained from the FISH kit (GenePharma, China). The FISH probe sequence of *hsa_circ_0005882* is listed in Supplementary Table S1.

Luciferase reporter assay. 293T cells were seeded into 6-well plates and cotransfected with wild type (WT) or mutant (MUT) PRL-TK-pMIR-circ_0005882 and *miR-654-3p* mimics or mimics NC (negative control). After 48 h of incubation, seeding into 96-well plates, the Firefly and Renilla luciferase activities were measured with a dual-luciferase reporter assay (#DL101-01, Vazyme, China) and normalized to the Renilla luciferase activity.

Actinomycin D and RNase R treatment. Cells were treated with 6 μg/mL actinomycin D (#GC16866, GLPBIO, USA) and collected at the designated time point. For the RNase R treatment, total RNA (2 μg) was incubated for 20 min at 37 °C with 2 U/μg of RNase R (#GE10003, GLPBIO, USA). After the actinomycin D or RNase R treatment, the expression level of *circ_0005882* was analyzed by RT-qPCR.

RNA immunoprecipitation (RIP). Antibodies for RIP assays against YTHDF2 (#24744-1-AP) and IgG (#10284-1-AP) were purchased from Proteintech. Briefly, cells were harvested, lysed with RIP lysis buffer and incubated with magnetic beads and specific antibodies or IgG antibodies on a rotator overnight at 4 °C. After magnetic separation, the protein-RNA complexes were treated with proteinase K at 55 °C for 30 min. The released RNA was purified using TRIzol Reagent (#9108, Takara, Japan), followed by reverse transcription and subsequent qPCR analysis.

Methylated RNA immunoprecipitation qPCR (MeRIP-qPCR). This procedure was adapted from the published reports [23, 24]. Briefly, RNAs isolated from HNE1 cells was incubated with 5 μg of anti-m6A antibody (#202003, Synaptic Systems, Germany) or normal rabbit IgG in IP buffer (150 mM NaCl, 10 mM Tris-HCl, 0.1% NP-40, pH 7.4) containing RNase inhibitor at 4 °C for 2 h. Subsequently, protein A/G magnetic beads (#HY-K0202, Medchemexpress, USA) were added and incubation with rotation at 4 °C for 2 h. After washing, the captured RNAs were eluted via competitive displacement with IP buffer containing 6.7 mM m6A sodium salt (#HY-111926, Medchemexpress, USA) and concentrated by ethanol precipitation. Then, the RNAs were used for cDNA synthesis and qPCR analysis as previously described.

SELECT (Single-base elongation and ligation-based qPCR amplification). Specific positions of m6A modification on circ_0005882 were probed by single-base elongation and ligation-based

qPCR amplification (SELECT) as previously reported [25]. The SELECT primers were purchased from Sangon Biotech (China) and listed in Supplementary Table S3.

circRNA high-throughput sequencing. Total RNA was extracted from si-NC and si-YTHDF2 HNE1 cells using Magzol Reagent (#R4801-03, Magen, China) as per the manufacturer's instructions. After removal of ribosomal RNAs using the RiboCop rRNA Depletion Trial Kit (#K14496, LEXOGEN, Austria), the RNA was digested with RNase R (RNR07250, Epicentre, USA) and fragmented into ~200 bp fragments. The purified RNA fragments were then employed for first- and second-strand cDNA synthesis, followed by adapter ligation and low-cycle amplification according to the NEBNext® Ultra™ RNA Library Prep Kit for Illumina (#E7530L, NEB, USA) protocol. The quality of the libraries was evaluated using the Agilent 2200 TapeStation and Qubit (Thermo Fisher Scientific, USA). Subsequent sequencing was conducted on an Illumina platform with a paired-end 150 bp read length at Ribobio Co. Ltd (Ribobio, China). For circRNA identification, two algorithms, CIRI2 and CIRCexplorer2, were utilized. Reads were mapped to the human reference genome GRCh37/hg19 (http://genome.ucsc.edu/) via BWA-MEM or Tophat, respectively. Only circRNAs that were detected by both algorithms were considered reliably identified. A threshold of $|\log_2 FC| > 1$ and $p < 0.05$ was applied to identify differentially expressed circRNAs. The datasets presented in this study have been deposited in the Gene Expression Omnibus (GEO) repository under accession number GSE335362.

Sanger sequencing. RNA extracted from HNE1 cells was treated with RNase R and subsequently reverse-transcribed with random primers to generate cDNA. Circ_0005882 was amplified by PCR, followed by agarose gel electrophoresis, and the target band was excised and purified using a SanPrep Column DNA Gel Extraction Kit (#B518131, Sangon Biotech, China). The purified product was then ligated into a T-vector using the pMD™ 19-T Vector Cloning Kit (#6013, Takara, Japan). Selected colonies were subjected to Sanger sequencing (Sangon Biotech, China). Sanger sequencing was performed using the dideoxy chain-termination method, and the products were analyzed on a 3730×l DNA analyzer (Applied Biosystems, USA).

Statistical analysis. All experiments were performed at three times independently. Data are presented as the means±standard deviation (SD). Statistical significance between two groups was determined by Student's t-test, and three or more than three groups was assessed using one-way analysis of variance (ANOVA). P-value < 0.05 was considered statistically significant (*$p < 0.05$;

195 **p < 0.01; ***p < 0.001).

196

197

Results

Characterization of *circ_0005882*. In our research on the epigenetic mechanisms underlying the occurrence and development of NPC, a circRNA named *circ_0005882,* which is abnormally increased upon knockdown of the m6A-binding protein YTHDF2 followed by circRNA sequencing, has attracted our attention (Supplementary Figure S1, Supplementary Table S4). *circ_0005882* originates from back-splicing of exons 9-14 of the human *STK39* gene, resulting in a 402 nt circular transcript. Sanger sequencing showed that the PCR product of the circRNA corresponded to exon 9 to exon 14 of the *STK39* gene through head-to-tail splicing, matching the sequence reported for *circ_0005882* in circBase (Figure 1A). To verify the circular feature of *circ_0005882*, RT-qPCR assay was conducted using oligo (dT) and random primers in 5-8F and HNE1 NPC cell lines. The results showed that compared with random primers, *circ_0005882* expression was significantly reduced, while *GAPDH* expression did not change when using oligo (dT) primers, suggesting that *circ_0005882* contained no poly-A tail (Figure 1B). Further analysis showed that after treatment of RNase R, the RNA level of *STK39* was significantly reduced, whereas *circ_0005882* remained unchanged, indicating that *circ_0005882* resists RNase R digestion in both 5-8F and HNE1 cells (Figure 1C). These results indicate *circ_0005882* harbors a circular RNA structure. FISH assay was further performed to clarify the subcellular localization of *circ_0005882*. The results indicated that *circ_0005882* existed in both cytoplasm and nucleus in 5-8F and HNE1 cell lines with stable *circ_0005882* overexpression (Figure 1D). The localization of *circ_0005882* was also confirmed by cytoplasmic and nuclear fractionation assay (Figure 1E). These results indicated that *circ_0005882* is a real existing circular RNA present in both the cytoplasm and nucleus of NPC cells.

***circ_0005882* suppresses NPC cells proliferation.** We further investigated the expression and function of *circ_0005882* in NPC cells. RT-qPCR results indicated that *circ_0005882* expression was reduced in the NPC cell lines (5-8F and HNE1) relative to the immortalized normal nasopharyngeal epithelial cell line NP69 (Figure 2A). To analyze the function of *circ_0005882* in NPC, we transfected overexpression plasmids into 5-8F and HNE1 cells. The overexpression efficiency of *circ_0005882* in 5-8F and HNE1 cells was confirmed by RT-qPCR (Figures 2B, 2C). CCK-8 assay showed that overexpression of *circ_0005882* suppressed the cell viability of 5-8F and HNE1 (Figures 2D, 2E). EdU assay also revealed that overexpression of *circ_0005882* significantly restricted the proliferative capacity of 5-8F and HNE1 (Figures 2F-2I). Stable cell lines

overexpressing *circ_0005882* were generated in 5-8F cells (5-8F LV-circ_0005882) via lentiviral transduction (Figure 2J). Compared with the 5-8F LV-NC cell line, the 5-8F LV-circ_0005882 cell line displayed significantly inhibited proliferation. This inhibitory effect was reversed upon *circ_0005882* silencing (Figures 2K, 2L). These results indicated that *circ_0005882* suppresses NPC cells proliferation.

***circ_0005882* is identified as an m6A modified circRNA.** To identify potential regulatory mechanisms, we examine the sequence of *circ_0005882*. Bioinformatic analysis identified nine and six putative m6A modification sites using circPrimer and SRAMP (http://www.cuilab.cn/sramp), respectively, lending support to its potential regulation by m6A (Figures 3A, 3B). MeRIP-qPCR assay was performed to confirm the existence of m6A modification in *circ_0005882*. The results showed that *circ_0005882* was significantly enriched by the m6A antibody, indicating the existence of m6A modification in *circ_0005882* (Figure 3C). To find the specific modification sites, we conducted the single-base elongation- and ligation-based qPCR amplification method (SELECT), according to a previous report [25]. The consistent sites (16, 51, 86, 93, 168, and 354) in *circ_0005882* predicted by two prediction methods were detected. METTL3 is the pivotal enzyme that catalyzes m6A RNA modification, working as the active core of the methyltransferase complex to transfer a methyl group from S-adenosylmethionine to the N6 position of adenosine [26]. It has been demonstrated that METTL3 knockdown reduces m6A modification on circRNA [27]. When METTL3 was silenced in HNE1 cells, the SELECT product at the 51, 168, and 354 sites were increased, whereas the 16, 86, 93 sites and the non-m6A site were unaffected. This suggests that positions 51, 168, and 354 of *circ_0005882* may harbor m6A modifications (Figures 3D-3J).

YTHDF2 inhibited *circ_0005882* expression by downregulating its stability in an m6A-dependent manner. Given that circ_0005882 contains m6A modification, we further investigated the regulatory effect of m6A modification on *circ_0005882* in NPC. The results showed that knockdown of the key m6A methyltransferase METTL3 in 5-8F and HNE1 cell lines led to increased *circ_0005882* expression levels (Figures 4A, 4B). Several recent studies have suggested that despite their higher stability compared to linear RNAs, the expression of circRNAs is still subject to regulation by the m6A reader YTHDF2 via a mechanism that mediates their degradation [28-30]. Therefore, we further determined whether the increase in *circ_0005882* expression upon *METTL3* silencing was mediated by YTHDF2. Similarly, YTHDF2 knockdown led

to an elevation of *circ_0005882* levels in both 5-8F and HNE1 cells (Figures 4C, 4D). Considering that YTHDF2 acts as an m6A binding protein that primarily mediates its effects by recognizing m6A-modified RNAs and regulating their stability, we further investigated whether this mechanism underlies the inhibitory effect of YTHDF2 on *circ_0005882* expression. RIP-qPCR assay confirmed that YTHDF2 protein could bind *circ_0005882* (Figure 4E). Upon treatment with actinomycin D, overexpression of YTHDF2 decreased the stability of *circ_0005882* (Figure 4F). These results indicated that YTHDF2 downregulates *circ_0005882* expression by inhibiting its stability in an m6A-dependent manner.

YTHDF2 drives NPC cell proliferation via the regulation of *circ_0005882*. We further investigated the regulatory role of YTHDF2 in *circ_0005882* functional consequence on NPC cell proliferation. EdU assay demonstrated that overexpression of YTHDF2 significantly enhanced the proliferative capacity of HNE1 cells, whereas this pro-proliferative effect was largely abrogated upon co-expression of *circ_0005882* (Figures 5A, 5B). The functional rescue data suggested that downregulation of *circ_0005882* may be a critical mediator underlying YTHDF2-induced NPC cell proliferation.

***circ_0005882* acts as a sponge for *miR-654-3p* in NPC.** After identifying the YTHDF2-m6A-dependent regulation of *circ_0005882*, we investigated how it exerts its inhibitory effect on NPC progression. The primary regulatory mechanism of circRNAs involves their role as competing endogenous RNAs (ceRNAs), which function by sponging and sequestering miRNAs [31, 32]. To explore the miRNAs that could be sponged by *circ_0005882*, we integrated bioinformatic analysis including circinteractome and miRanda databases to predict its downstream miRNA targets (Figure 6A). From the pool of nine miRNAs overlapping in the two datasets, *miR-654-3p* was identified for further study due to its predicted favorable binding relationship with the circ_0005882 (Figure 6C) and high scores (miRanda score=148; circinteractome context+score percentile=98). RT-qPCR results showed that *circ_0005882* overexpression significantly inhibited *miR-654-3p* level (Figure 6B). The wild-type (*circ_0005882*-WT) and mutant (*circ_0005882*-MUT) luciferase reporter plasmids were constructed based on the binding relationship between *circ_0005882* and *miR-654-3p* (Figure 6C). The luciferase reporter assay showed that the luciferase activity of *circ_0005882*-WT but not the mutant was significantly reduced by *miR-654-3p* mimics (Figure 6D). These results demonstrate that *circ_0005882* functions as a molecular sponge to absorb

and inhibit *miR-654-3p*.

YTHDF2/*circ_0005882/miR-654-3p axis* contributes to NPC proliferation. To investigate the effects of YTHDF2/*circ_0005882*/*miR-654-3p* axis in NPC, a series of functional rescue experiments were performed. The results demonstrated that overexpression of *miR-654-3p* in HNE1 LV- *circ_0005882* cells can reverse the inhibitory effects of *circ_0005882* on cells proliferation (Figures 7A, 7B). On the other hand, *miR-654-3p* inhibitor can reverse the promotive effect of YTHDF2 on 5-8F cell proliferation (Figures 7C, 7D). These results suggest that the mechanism by which YTHDF2 promotes NPC proliferation may partially involve the upregulation of *miR-654-3p* via the suppression of *circ_0005882*. Therefore, our research suggests that *circ_0005882* functions as a sponge for *miR-654-3p* to inhibit NPC proliferation. m6A reader YTHDF2 promotes the degradation of *circ_0005882* by recognizing its m6A sites, resulting in the release of sequestered *miR-654-3p* and subsequent proliferation of NPC cells (Figure 8).

Discussion

In recent years, the role of circRNAs in the occurrence and development of tumors has attracted increasing attention. Unlike linear RNAs, circRNAs are resistant to degradation by exonucleases like RNase R due to their closed-loop structure, which underlies their high stability. *Circ_0005882* attracted our attention due to its abnormally altered in YTHDF2-knockdown HNE1 cells, as well as the presence of multiple predicted m6A sites. Using Sanger sequencing and RNase digestion assays, we confirmed that *circ_0005882* harbors a circular structure. Accumulating evidence establishes circRNAs as key regulators regulating the tumorigenesis and progression of multiple cancer types. However, the effects of circRNA vary in different tumors. For example, in gastric cancer, *circMRPL35* enhances cell motility and invasion by sponging *miR-6809-3p* and upregulating ZNF90, primarily through modulating the epithelial-mesenchymal transition (EMT) process and the TGF-β1/SMAD2/3 signaling pathway [7]. *CircZFAND6* exerted tumor-suppressive effects by inhibiting cellular proliferation, migration, and invasion, which was achieved through its regulation of the *miR-6815-3p*/APC/Wnt-β-catenin pathway in gastric cancer [10]. In NPC, the *circSETD3*/PDIA6 axis enhances tumor cell survival under radiotherapeutic stress by mitigating ER stress. Specifically, *circSETD3* binds to and stabilizes *PDIA6* mRNA, upregulating its protein level, maintaining ER proteostasis and suppresses the unfolded protein response (UPR) [11]. *CircCLASP2*

acted as a molecular scaffold that facilitated the approximation of DExH-Box Helicase 9 (DHX9) to protein-L-isoaspartate (D-aspartate) O-methyltransferase 1 (*PCMT1*) mRNA, leading to upregulation of cytoskeleton-associated proteins, and ultimately driving NPC cell proliferation and metastasis [33]. Yang et al. [34] employed circRNA high-throughput sequencing to delineate the circRNA expression profiles in four NPC patients and four healthy controls. Their analysis revealed a total of 93 upregulated and 77 downregulated circRNAs. *circ_0005882* was detected in all examined samples, although no significant difference was observed between the two groups, confirming the objective existence of this circular RNA in both NPC tissue and nasopharyngeal epithelial tissue. Our study found that, compared to NP69 nasopharyngeal epithelial cells, the expression of *circ_0005882* in NPC cell lines HNE1 and 5-8F is downregulated. Whether these discrepancies are attributable to genetic differences between clinical specimens and NPC cell lines, or to the modulatory effects of the tumor microenvironment present in clinical samples on *circ_0005882* expression, warrants further investigation. Our study found that *circ_0005882* exerted a tumor-suppressive role in NPC by effectively inhibiting 5-8F and HNE1 cells proliferation. Several recent studies have elaborated on the mechanisms of tumor-suppressive circular RNAs in NPC. For example, *circCCNB1* competitively binds to nuclear factor 90 (NF90), blocking its interaction with *pri-miR-7-1* and *pri-miR-15b*, thereby enhancing DGCR8-mediated production of mature *miR-7-1-3p* and *miR-15b-5p*. These miRNAs repress the expression of calumenin (*CALU*), kinesin family member 1B (*KIF1B*), and RNA polymerase III subunit G (*POLR3G*), downregulate vasculogenic mimicry (VM) markers, and suppress VM in NPC cells [35]. Additionally, *circCCNB1* also inhibits NPC cell migration and invasion by simultaneously binding to NF90 protein and tight junction protein 1 (*TJP1*) mRNA, thereby enhancing *TJP1* mRNA stability [36]. Wang et al. [37] demonstrated that *circTP63-N* exerts tumor-suppressive functions in NPC by interacting with HSP90AB1, leading to the recruitment of LATS/YAP1 proteins and driving the phosphorylation- and ubiquitination-dependent degradation of YAP1, ultimately suppressing NPC proliferation and metastasis. Our discovery of the function of *circ_0005882* further enriches the regulatory network of tumor-suppressive circRNAs in NPC.

circRNAs exert their functional roles through diverse molecular mechanisms, including: functioning as competitive endogenous RNAs (ceRNAs) to sponge miRNAs; modulating protein activity or localization through direct interactions; regulating the transcription of their host genes;

and encoding functional peptides [38]. An increasing number of studies indicate that the ceRNA mechanism has emerged as the important mechanism underlying circRNA functionality in NPC. Ma et al. [39]. revealed that *circ_CIT* promoted NPC progression by sponging *miR-409-3p* to upregulate ZEB1, which enhanced tumor cell proliferation and metastasis and drove macrophage M2 polarization. Hong et al. [40] demonstrated that overexpression of *circCRIM1* enhanced NPC cell metastasis and EMT by competitively sponging *miR-422a*, thereby preventing *miR-422a* from suppressing its target forkhead box Q1 (*FOXQ1)*. *CircCTDP1* sequesters *miR-320b*, leading to the upregulation of homeobox A10 (*HOXA10*), which in turn drives NPC progression [41]. In this study, we also found that *circ_0005882* exerts its inhibitory effect on NPC proliferation through the mechanism of sponging miRNA. Luciferase assay results validated the ceRNA mechanism of *circ_0005882*, demonstrating its ability to sequester *miR-654-3p*. *miR-654-3p* has been found to exhibit dual roles in tumor progression, acting as both a tumor suppressor or an oncogene. Wang et al. [42] demonstrate that by directly binding to and repressing *miR-654-3p*, *LINC00885* relieves the suppression on *miR-654-3p* target SLBP, activating the PI3K/Akt signaling pathway, ultimately promoting lung squamous cell carcinoma (LUSC) progression. AlkB homolog 5 (ALKBH5) enhanced the stability and expression of *NEAT1*, facilitating head and neck squamous cell carcinoma (HNSCC) progression by modulating the *miR-654-3p*/HOXA10 axis [43]. A study reported that *circEFR3A* acted as a *miR-654-3p* sponge to facilitate the proliferation and migration of NPC cell lines C666-1 and SUNE1. This competitive binding upregulated EFR3 homolog A *(EFR3A),* driving oncogenic phenotypes [44]. On the other hand, some research has indicated an oncogenic role for *miR-654-3p*. Deng et al. [45] demonstrate that *miR-654-3p* could enhance the growth of AGS and HGC27 gastric cancer (GC) cell lines. They identify p21 is a target of *miR-654-3p*. *CircRHOBTB3* acted as a ceRNA for oncogenic *miR-654-3p*, thereby promoting p21 expression and inhibiting tumor growth. *Circ_0067514* suppresses GC progression and glycolysis by targeting the *miR-654-3p*/LATS2 axis [46]. Chen et al. [47] found that while lncRNA EMX2 opposite strand/antisense RNA (EMX2OS) suppressed tumor cell growth, migration, invasion, and induced apoptosis, *miR-654-3p* overexpression conversely abolished these EMX2OS-mediated effects. Our study indicates that *circ_0005882* exerts inhibitory effect on proliferation of 5-8F and HNE1 NPC cell lines by adsorbing *miR-654-3p*, suggesting that *miR-654-3p* is a pro-proliferative factor, at least in the 5-8F and HNE1 cell lines. These differences might be attributed to the

complex genetic profiles of different cell lines, a possibility that requires future study.

The m6A modification represents the predominant form of internal RNA methylation in eukaryotes. In recent years, an increasing number of circRNAs have been found to undergo m6A modification. Li et al. [22] demonstrated that *circNEK11*, modified by m6A and exported to the cytoplasm via YTH N6-methyladenosine RNA binding protein C1 (YTHDC1), promoted hepatocellular carcinoma (HCC) progression and recurrence by sponging *miR-1236-3p* to upregulate GPX2 expression. Another study revealed that m6A-modified *cLMNB1* overcame osimertinib resistance in lung adenocarcinoma (LUAD) by destabilizing the fibroblast growth factor receptor 4 (FGFR4) protein, which highlights the therapeutic potential of *cLMNB1* with an m6A modification site mutation as a novel nucleic acid agent [48]. Our study confirmed that *circ_0005882* may harbor m6A modification sites and YTHDF2 promotes its instability. Similar to our findings, recent studies have shown that YTHDF2 can diminish the stability and biological functions of circRNAs. Park et al. [28] demonstrated that the m6A reader YTHDF2 recognizes m6A-modified circRNAs and recruits the RNase P/MRP and HRSP12 complex, thereby mediating their cleavage and subsequent degradation. Chen et al. [29] found that YTHDF2 recognized the m6A-modified *circIRF2* and impaired its stability, thereby relieving the *circIRF2*-mediated competitive sequestration of *miR-29b-1-5p*, inhibiting forkhead box O3 (FOXO3) nuclear translocation and ultimately promoting liver fibrosis. In colorectal cancer (CRC), Chen et al. [30] reported that the decreased level of *circ_0003215* resulted from m6A-mediated RNA degradation by the reader protein YTHDF2. Acting through the miR-663b/DLG4/G6PD axis, *circ_0003215* was identified as a key regulator that curbs metabolic glucose reprogramming and inhibits tumor growth and progression. Yu et al. [49] recently demonstrated that in the NPC cell lines 5-8F and CNE1, overexpression of YTHDF2 suppressed FOXO1 expression by reducing its stability and promoting its degradation and thereby promoted malignant behavior in NPC. Interestingly, the ENCORI database [50] (https://rnasysu.com/encori) identifies *FOXO1* as a putative target of *miR-654-3p*. Given our observation that YTHDF2 suppresses *circ_0005882*, thereby liberating *miR-654-3p*, we speculate that YTHDF2 may also downregulate FOXO1 by enhancing *miR-654-3p*-mediated targeting of *FOXO1* mRNA. Nevertheless, further experimental investigation is needed to substantiate this possibility.

This study has several limitations. First, the specific target genes of *miR-654-3p* have not been

identified. Second, EBV plays a critical role in the development of NPC, but our current experimental model does not account for the context of EBV infection. Future studies should incorporate this important factor. Third, our study is limited to in vitro experiments and lacks in vivo validation, which awaits further investigation. Despite these limitations, our article also reports several important findings. We constructed a regulatory YTHDF2/*circ_0005882*/*miR-654-3p* axis that plays an important role in NPC proliferation. YTHDF2 promotes NPC cell proliferation by suppressing *circ_0005882*, thereby relieving *circ_0005882* inhibitory constraint on *miR-654-3p*. The identification of this regulatory axis provides novel mechanistic insight into NPC pathogenesis and, more importantly, pinpoints a targetable m6A-circRNA-miRNA network with therapeutic potential. These results suggest that *circ_0005882* with m6A site mutations may have important clinical application value in the treatment of NPC.

Acknowledgements: The authors thank Dr. Jian Ma and Xiaoyue Zhang (Central South Univ.) for providing technical help, reagents and cell lines.

The article has been supported by the National Natural Science Foundation of China (No. 82460464), Guangxi Science and Technology Program Project (China) (No. AD23026251) and Guangxi Natural Science Foundation (China) (No.2020GXNSFBA297082).

Supplementary data are available in the online version of the paper.

References

[1] CHEN YP, CHAN ATC, LE QT, BLANCHARD P, SUN Y et al. Nasopharyngeal carcinoma. Lancet 2019; 394: 64-80. https://doi.org/10.1016/S0140-6736(19)30956-0

[2] TANG LL, CHEN WQ, XUE WQ, HE YQ, ZHENG RS et al. Global trends in incidence and mortality of nasopharyngeal carcinoma. Cancer Lett 2016; 374: 22-30. https://doi.org/10.1016/j.canlet.2016.01.040

[3] LEE J, ROH JL. Targeting Ferroptosis in Nasopharyngeal Carcinoma: Mechanisms, Resistance, and Precision Therapeutic Opportunities. Int J Mol Sci 2025; 26: 11439. https://doi.org/10.3390/ijms262311439

[4] DAI Q, YUAN X, DONG H, XUE H. From immune suppression to immunotherapy sensitization: the dual roles of circRNAs in cancer progression. Front Immunol 2025; 16: 1723383. https://doi.org/10.3389/fimmu.2025.1723383

[5] LI J, ZHANG L, WANG Y, LI C. Dual-faced circRNAs: orchestrating immunosuppression and activation in the lung cancer microenvironment. Front Cell Dev Biol 2025; 13: 1706393. https://doi.org/10.3389/fcell.2025.1706393

[6] VAN ZONNEVELD AJ, KOLLING M, BIJKERK R, LORENZEN JM. Circular RNAs in kidney disease and cancer. Nat Rev Nephrol 2021; 17: 814-826. https://doi.org/10.1038/s41581-021-00465-9

[7] WANG X, YAO Z, LIU Y, MAO B, SHAO C et al. circMRPL35 promotes gastric cancer progression through the miR-6809-3p/ZNF90 axis and affects the EMT process and TGF-beta1/SMAD2/3 signaling. Noncoding RNA Res 2026; 16: 79-92. https://doi.org/10.1016/j.ncrna.2025.10.002

[8] ZHOU ZH, WEN JH, ZHANG YZ, YAO K, LI ZY et al. Mitochondria-located circRCP regulates redox homeostasis via stabilizing LRPPRC/SLIRP complex to promote bladder urothelial carcinoma tumorigenesis. Cancer Lett 2026; 638: 218157. https://doi.org/10.1016/j.canlet.2025.218157

[9] XIA Z, LIU W, GUO D, CHEN L, ZHAO M et al. circADAMTS12 Inhibits the Antitumor Activity of Microglia to Enable Metastatic Colonization in the Brain. Cancer Res 2025; 85: 4977-4994. https://doi.org/10.1158/0008-5472.CAN-25-0738

[10] DENG ZJ, OUYANG LY, GUO JP, YAO HT, LIU JJ et al. CircZFAND6 suppresses gastric cancer metastasis and reduces resistance to TKI therapy. Mol Cancer 2025; 24: 305. https://doi.org/10.1186/s12943-025-02478-5

[11] XIANG P, TANG L, ZHANG Y, MENDOZA JJ, YAN Q et al. circSETD3 confers radiotherapy resistance in nasopharyngeal carcinoma by attenuating ER stress-induced autophagy and apoptosis via PDIA6 upregulation. Oncogene 2026; 45: 368-382. https://doi.org/10.1038/s41388-025-03652-1

[12] MAO Z, WANG B, ZHANG T, CUI B. The roles of m6A methylation in cervical cancer: functions, molecular mechanisms, and clinical applications. Cell Death Dis 2023; 14: 734. https://doi.org/10.1038/s41419-023-06265-2

[13] FENG T, LIN L, ZHOU X, LI L, CHEN Y et al. CAP1-Mediated m6A modification of RRM2 suppresses tumor-associated M2 macrophage polarization and colorectal cancer growth. Cell Mol Life Sci 2026; 83: 64. https://doi.org/10.1007/s00018-025-06031-x

[14] Zhang X, Zhang Y, Liu X, Liu C, Liu Y et al. FOCAS: Transcriptome-wide screening of individual m(6)A sites functionally dissects epitranscriptomic control of gene expression in cancer. Cell 2026; 189: 922-938.e923. https://doi.org/10.1016/j.cell.2025.11.037

[15] XIE Y, LI Y, TANG M, LI Z, HU W et al. The BRAF V600E/MEK/ERK/METTL3 positive feedback loop regulates autophagy and promotes stemness and invasiveness in glioblastoma via m(6)A modification. J Exp Clin Cancer Res 2025; 45: 28. https://doi.org/10.1186/s13046-025-03623-0

[16] Zhang W, Lin J, Zhou Y, Wu C, Li Q et al. TNF-alpha-driven m6A modification disrupts the immunoregulatory function of MSCs by regulating HDAC5-dependent super-enhancers. Cell Death Dis 2025; 16: 902. https://doi.org/10.1038/s41419-025-08192-w

[17] TANG D, CAO C, HUANG S, HE Q, WANG A. YTHDF2 drives oral squamous cell carcinoma progression via m(6)A-dependent degradation of MTUS1/ATIP1 mRNA and mitochondrial dysregulation. Cell Signal 2025; 136: 112145. https://doi.org/10.1016/j.cellsig.2025.112145

[18] WANG X, LU Z, GOMEZ A, HON GC, YUE Y et al. N6-methyladenosine-dependent regulation of messenger RNA stability. Nature 2014; 505: 117-120. https://doi.org/10.1038/nature12730
[19] YANG S, CUI YH, LI H, WEI J, PARK G et al. YTHDF2 regulates self non-coding RNA metabolism to control inflammation and tumorigenesis. Nat Commun 2025; 16: 9946. https://doi.org/10.1038/s41467-025-64898-7
[20] JIN X, LV Y, BIE F, DUAN J, MA C et al. METTL3 confers oxaliplatin resistance through the activation of G6PD-enhanced pentose phosphate pathway in hepatocellular carcinoma. Cell Death Differ 2025; 32: 466-479. https://doi.org/10.1038/s41418-024-01406-2
[21] MA C, WANG D, GAO W, WANG X, XU X et al. METTL3-mediated m6A modification of circCDYL promotes gastric cancer progression by acting as miR-378a-5p sponge to regulate USP13 expression. Cell Signal 2026; 138: 112244. https://doi.org/10.1016/j.cellsig.2025.112244
[22] LI Q, HUANG X, TONG Y, YONG C, SONG M et al. et al: N6-Methyladenosine-Modified circNEK11 Promotes Hepatocellular Carcinoma Progression via the miR-1236-3p/GPX2 Axis. Cancer Sci 2025; 116: 3326-3336. https://doi.org/10.1111/cas.70203
[23] DOMINISSINI D, MOSHITCH-MOSHKOVITZ S, SALMON-DIVON M, AMARIGLIO N, RECHAVI G. Transcriptome-wide mapping of N(6)-methyladenosine by m(6)A-seq based on immunocapturing and massively parallel sequencing. Nat Protoc 2013; 8: 176-189. https://doi.org/10.1038/nprot.2012.148
[24] ZHENG Q, HOU J, ZHOU Y, LI Z, CAO X. The RNA helicase DDX46 inhibits innate immunity by entrapping m(6)A-demethylated antiviral transcripts in the nucleus. Nat Immunol 2017; 18: 1094-1103. https://doi.org/10.1038/ni1217-1361a
[25] XIAO Y, WANG Y, TANG Q, WEI L, ZHANG X et al. An Elongation- and Ligation-Based qPCR Amplification Method for the Radiolabeling-Free Detection of Locus-Specific N(6) -Methyladenosine Modification. Angew Chem Int Ed Engl 2018; 57: 15995-16000. https://doi.org/10.1002/anie.201807942
[26] DONG Y, LIU Y, MARCIANO D, NEFZI A, BLACK SM et al. The Emerging Role of METTL3 in Lung Diseases. Int J Mol Sci 2025; 27: 85. https://doi.org/10.3390/ijms27010085
[27] JI Y, ZHAO Q, FENG W, PENG Y, HU B et al. N6-Methyladenosine Modification of CIRCKRT17 Initiated by METTL3 Promotes Osimertinib Resistance of Lung Adenocarcinoma by EIF4A3 to Enhance YAP1 Stability. Cancers (Basel) 2022; 14: 5582. https://doi.org/10.3390/cancers14225582
[28] PARK OH, HA H, LEE Y, BOO SH, KWON DH et al. Endoribonucleolytic Cleavage of m(6)A-Containing RNAs by RNase P/MRP Complex. Mol Cell 2019; 74: 494-507.e498. https://doi.org/10.1016/j.molcel.2019.02.034
[29] CHEN X, ZHU S, LI HD, WANG JN, SUN LJ et al. N(6)-methyladenosine-modified circIRF2, identified by YTHDF2, suppresses liver fibrosis via facilitating FOXO3 nuclear translocation. Int J Biol Macromol 2023; 248: 125811. https://doi.org/10.1016/j.ijbiomac.2023.125811
[30] CHEN B, HONG Y, GUI R, ZHENG H, TIAN S et al. N6-methyladenosine modification of circ_0003215 suppresses the pentose phosphate pathway and malignancy of colorectal cancer through the miR-663b/DLG4/G6PD axis. Cell Death Dis 2022; 13: 804. https://doi.org/10.1038/s41419-025-08199-3

[31] LIU L, GU M, MA J, WANG Y, LI M et al. CircGPR137B/miR-4739/FTO feedback loop suppresses tumorigenesis and metastasis of hepatocellular carcinoma. Mol Cancer 2022; 21: 149. https://doi.org/10.1186/s12943-022-01619-4

[32] WANG Y, FU R, CHEN Y, WANG Y, YU Y et al. Hsa_circ_PCNT sponges hsa-miR-133b to promote SHH medulloblastoma via TAGLN2. Cell Mol Life Sci 2026; 83: 62. https://doi.org/10.1007/s00018-025-06048-2

[33] PENG M, ZHANG S, WU P, HOU X, WANG D et al. Circular RNA circCLASP2 promotes nasopharyngeal carcinoma progression through binding to DHX9 to enhance PCMT1 translation. Mol Cancer 2025; 24: 67. https://doi.org/10.1186/s12943-025-02272-3

[34] YANG J, GONG Y, JIANG Q, LIU L, LI S et al. Circular RNA Expression Profiles in Nasopharyngeal Carcinoma by Sequence Analysis. Front Oncol 2020; 10: 601. https://doi.org/10.3389/fonc.2020.00601

[35] FAN C, TAN F, WU J, ZENG Z, GUO W et al. CircCCNB1 inhibits vasculogenic mimicry by sequestering NF90 to promote miR-15b-5p and miR-7-1-3p processing in nasopharyngeal carcinoma. Mol Oncol 2025; 19: 1876-1893. https://doi.org/10.1002/1878-0261.13821

[36] ZHAO M, WANG Y, TAN F, LIU L, HOU X et al. Circular RNA circCCNB1 inhibits the migration and invasion of nasopharyngeal carcinoma through binding and stabilizing TJP1 mRNA. Sci China Life Sci 2022; 65: 2233-2247. https://doi.org/10.1007/s11427-021-2089-8

[37] WANG D, ZUO S, GE J, QU H, WU J et al. circTP63-N suppresses the proliferation and metastasis of nasopharyngeal carcinoma via engaging with HSP90AB1 to modulate the YAP1/Hippo signaling pathway. Sci China Life Sci 2025; 68: 689-705. https://doi.org/10.1007/s11427-023-2737-2

[38] MA A, YANG Y, LU L, ZHANG Y, ZHANG X et al. Emerging roles of circular RNAs in nasopharyngeal carcinoma: functions and implications. Cell Death Discov 2024; 10: 192. https://doi.org/10.1038/s41420-024-01964-x

[39] MA C, CHEN J, ZHU C, WANG J, HUANG S et al. Circ_CIT Promotes Nasopharyngeal Carcinoma Progression and Macrophage M2 Polarization Through miR-409-3p/ZEB1 Axis. Cancer Manag Res 2025; 17: 1689-1705. https://doi.org/10.2147/CMAR.S526022

[40] HONG X, LIU N, LIANG Y, HE Q, YANG X et al. Circular RNA CRIM1 functions as a ceRNA to promote nasopharyngeal carcinoma metastasis and docetaxel chemoresistance through upregulating FOXQ1. Mol Cancer 2020; 19: 33. https://doi.org/10.1186/s12943-020-01149-x

[41] LI H, YOU J, XUE H, TAN X, CHAO C. CircCTDP1 promotes nasopharyngeal carcinoma progression via a microRNA- 320b/HOXA10/TGFbeta2 pathway. Int J Mol Med 2020; 45: 836-846. https://doi.org/10.3892/ijmm.2020.4467

[42] WANG L, HE X, XI Z, LI W, WEI L et al. LINC00885 promotes lung squamous cell carcinoma by upregulating SLBP expression to activate PI3K/Akt pathway. Clin Exp Med 2025; 25: 329. https://doi.org/10.1007/s10238-025-01863-0

[43] ZHANG S, BAI Y, WANG B, JU H. ALKBH5 Accelerates the Progression of Head and Neck Squamous Cell Carcinoma by Decreasing Methylation of the lncRNA NEAT1. Appl Biochem Biotechnol 2026; 198: 1635-1655. https://doi.org/10.1007/s12010-025-05517-5

[44] JIANG P, XIA B. Circular RNA EFR3A promotes nasopharyngeal carcinoma progression through modulating the miR-654-3p/EFR3A axis. Cell Mol Biol (Noisy-le-grand) 2023; 69: 111-117. https://doi.org/10.14715/cmb/2023.69.12.18

[45] DENG G, MOU T, HE J, CHEN D, LV D et al. Circular RNA circRHOBTB3 acts as a sponge for miR-654-3p inhibiting gastric cancer growth. J Exp Clin Cancer Res 2020; 39: 1. https://doi.org/10.1186/s13046-019-1487-2
[46] JIANG SF, LI RR. hsa_circ_0067514 suppresses gastric cancer progression and glycolysis via miR-654-3p/LATS2 axis. Neoplasma 2022; 69: 1079-1091. https://doi.org/10.4149/neo_2022_220225N209
[47] CHEN ZH, CUI MY, ZHANG HM. EMX2OS Delays Wilms'Tumor Progression via Targeting miR-654-3p. Ann Clin Lab Sci 2022; 52: 12-20.
[48] QIAN Y, WANG H, FENG Y, ZHANG Y, HU Q et al. The N6-methyladenosine-mediated cLMNB1 degrades FGFR4 to overcome osimertinib resistance in non-small cell lung cancer. Cell Death Dis 2025; 16: 818. https://doi.org/10.1038/s41419-025-08124-8
[49] YU P, WEI W, PENG X, YE J, JI Y et al. YTHDF2 enhances proliferation and metastasis of nasopharyngeal carcinoma by mediating m6A modification in destabilizing FOXO1 mRNA. Cancer Biol Ther 2025; 26: 2582349. https://doi.org/10.1080/15384047.2025.2582349
[50] ZHOU K, HUANG J, LIU S, ZHENG W, LIU S et al. An encyclopedic regulatory and functional atlas of RNA interactomes. Nat Methods 2026; 23: 1109-1114. https://doi.org/10.1038/s41592-026-03105-x

Figure Legends

Figure 1. Characterization of *circ_0005882*. A) The schematic diagram of genomic location of *circ_0005882*. The back-splicing of exons 9-14 of *STK39* gene to form *circ_0005882* was identified by Sanger sequencing. The green arrow and red arrow denote the location and orientation of primers spanning the *circ_0005882* splice junction. B) Relative levels of *circ_0005882* and GAPDH were determined by qPCR using oligo (dT) and random primers. C) Relative levels of *circ_0005882* and *STK39* mRNA in 5-8F and HNE1 cells were determined by qPCR after treatment with RNase R. D) FISH assay was used to determine subcellular localization of *circ_0005882* in stably *circ_0005882*-expressing 5-8F and HNE1 cell lines. Nuclei were stained with DAPI (blue), and *circ_0005882* was detected with specific probes (red). Scale bar, 10 μm. E) qPCR analysis to determine the subcellular localization of *circ_0005882* in 5-8F and HNE1 cells employing cytoplasmic and nuclear fractionation assay. Abbreviation: ns-not significant; ***$p < 0.001$ compared with the control group

Figure 2. *circ_0005882* suppresses the proliferation of NPC cells. A) The expression of *circ_0005882* in NP69, 5-8F and HNE1 cells were determined by qPCR. B, C) 5-8F, and HNE1 cells were transfected with either empty vector or *circ_0005882* overexpression vector

(OE-circ_0005882). The *circ_0005882* level was analyzed by qPCR. D, E) The proliferation of 5-8F (D) and HNE1 (E) cells transfected with empty vector or OE-circ_0005882 was analyzed by CCK-8 analysis. F, G) The proliferation of 5-8F (F) and HNE1 (G) cells transfected with empty vector or OE-circ_0005882 was analyzed by EdU analysis. Scale bar, 300 μm. The quantification of EdU positive cells in (F) and (G) were shown in (H) and (I), respectively. J) The expression of *circ_0005882* in stably *circ_0005882*-expressing 5-8F cell line (5-8F LV-circ_0005882) and the control cell line (5-8F LV-NC) were determined by qPCR. K) The cell proliferative activity of LV-NC transfected with si-NC, LV-circ_0005882 transfected with si-NC and LV-circ_0005882 transfected with si-*circ_0005882* were determined by EdU assays. Scale bar, 300 μm. The quantification of EdU positive cells in (K) was shown in (L). *$p < 0.05$; **$p < 0.01$; ***$p < 0.001$ compared with the control group.

Figure 3. *circ_0005882* is a m6A-modified circRNA in NPC cells. m6A modification sites in *circ_0005882* were predicted by circPrimer (A) and SRAMP (B). C) MeRIP-qPCR assay was used to determine the level of *circ_0005882* enriched by the m6A antibody. D) Stably *circ_0005882*-expressing HNE1 cells (HNE1 LV-circ_0005882) were transfected with siNC or siMETTL3. The expression of METTL3 was determined by qPCR. E-J) Relative SELECT products after performing SELECT method were determined by qPCR using pairs of primers designed for non-m6A control sites and each of the m6A sites (16, 51, 86, 93, 168 and 354). Abbreviation: ns-not significant; **$p < 0.01$; ***$p < 0.001$ compared with the control group

Figure 4. YTHDF2 inhibited *circ_0005882* expression by downregulating its stability in NPC cells. A, B) The RNA levels of *METTL3* and *circ_0005882* were determined by qPCR in 5-8F (A) and HNE1 (B) cells transfected with siNC and siMETTL3. C, D) The RNA levels of *YTHDF2* and *circ_0005882* were determined by qPCR in5-8F (C) and HNE1 (D) cells transfected with siNC and siYTHDF2. E) The interaction between YTHDF2 and *circ_0005882* in HNE1 cells was analyzed by RIP-qPCR assays. F) The level of *circ_0005882* exposed to actinomycin D treatment at the indicated time points in HNE1 cells was determined by qPCR. *$p < 0.05$; **$p < 0.01$; ***$p < 0.001$ compared with the control group

Figure 5. YTHDF2 promotes NPC cell proliferation via the regulation of *circ_0005882*. (A) HNE1 cells were transferred with OE-Ctrl + empty vector, OE-YTHDF2+empty vector, and OE-YTHDF2 + OE *circ_0005882* respectively. Cell proliferation was determined by EdU assay. Scale bar, 300 μm. (B) represents the quantification of EdU positive cells in (A). *$p < 0.05$; **$p < 0.01$ compared with the control group

Figure 6. *circ_0005882* acts as a sponge for *miR-654-3p*. A) Potential miRNAs candidates may bind to *circ_0005882* were predicted by circinteractome (green), TargetScan (blue), and miRanda (red) databases. B) Relative level of *miR-654-3p* in HNE1 cells transfected with empty vector and OE-circ_0005882 was determined by qPCR. C) Putative *miR-654-3p* binding site in *circ_0005882*. The potential complementary residues are shown in black vertical lines. Mutant bases are in red. D) 293T cells were cotransfected with wild type (WT) or mutant (MUT) PRL-TK-pMIR-circ_0005882 and miR-654-3p mimics or mimics NC. The Firefly and Renilla luciferase activities were measured with a dual-luciferase reporter assay and normalized to the Renilla luciferase activity. ns, not significant; ***$p < 0.001$ compared with the control group

Figure 7. YTHDF2/*circ_0005882/ miR-654-3p* axis regulates the proliferation of NPC cells. A) EdU assay was used to analyze cell proliferation of HNE1 LV-NC transfected with mimics NC, LV-circ_0005882 transfected with mimics NC and LV-circ_0005882 transfected with *miR-654-3p* mimics groups. Scale bar, 300 μm. The quantification of EdU positive cells in (A) was shown in (B). C) 5-8F cells were transfected with OE-Ctrl + inhibitor NC, OE-YTHDF2 + inhibitor NC, and OE-YTHDF2+miR654-3p inhibitor. Cell proliferation was determined by EdU assay. The quantification of EdU positive cells in (C) was shown in (D). **$p < 0.01$; ***$p < 0.001$ compared with the control group.

Figure 8. Diagram illustrating the mechanism by which YTHDF2/*circ_0005882/miR-654-3p* axis regulates NPC proliferation. Briefly, by recognizing the m6A sites on *circ_0005882*, YTHDF2 promotes *circ_0005882* degradation, which leads to the inhibition of adsorbing oncogenic *miR-654-3p*, subsequently promoting the proliferation of NPC cells.

Fig. 1 [Download full resolution image]

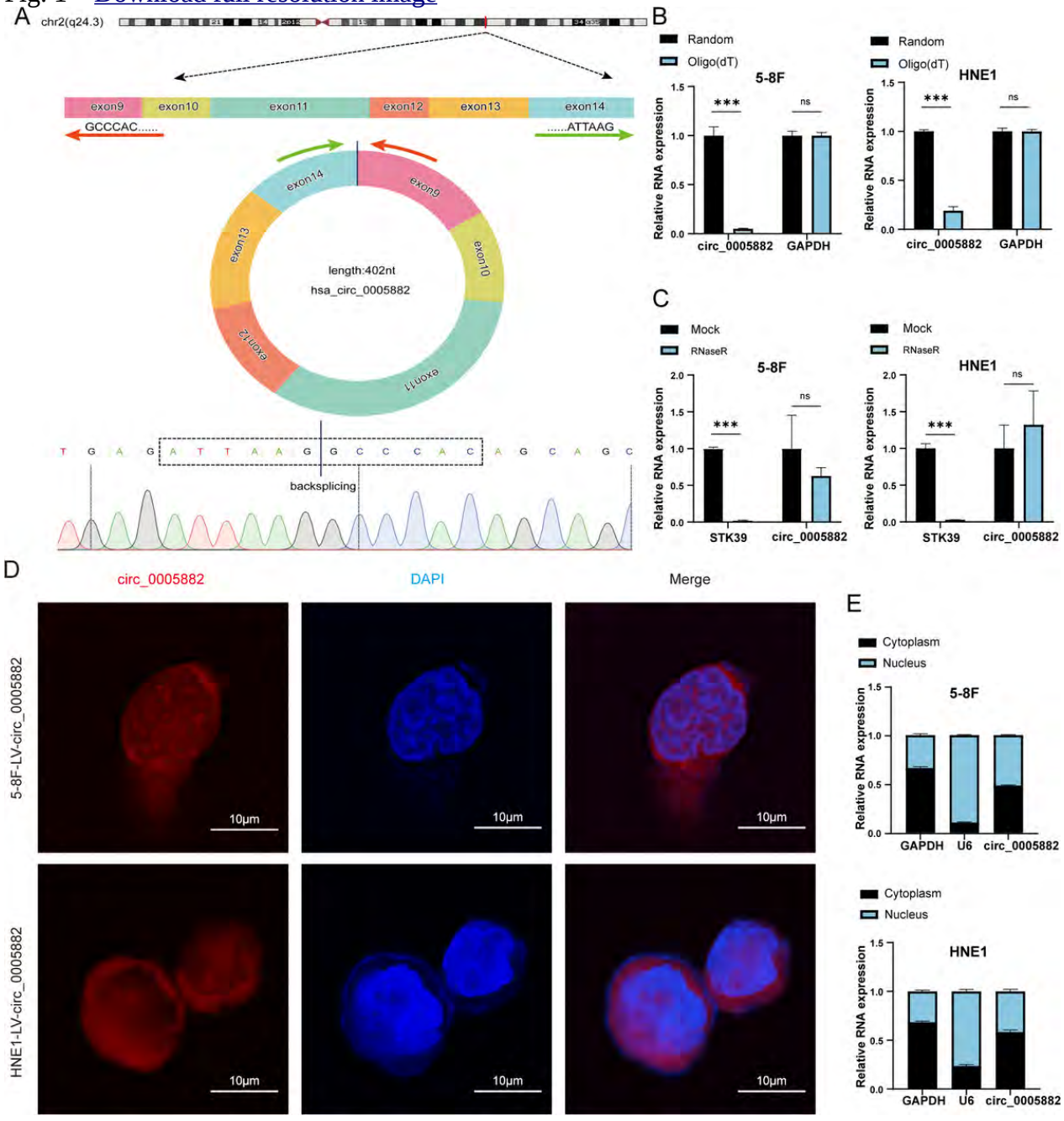

Fig. 2 [Download full resolution image]

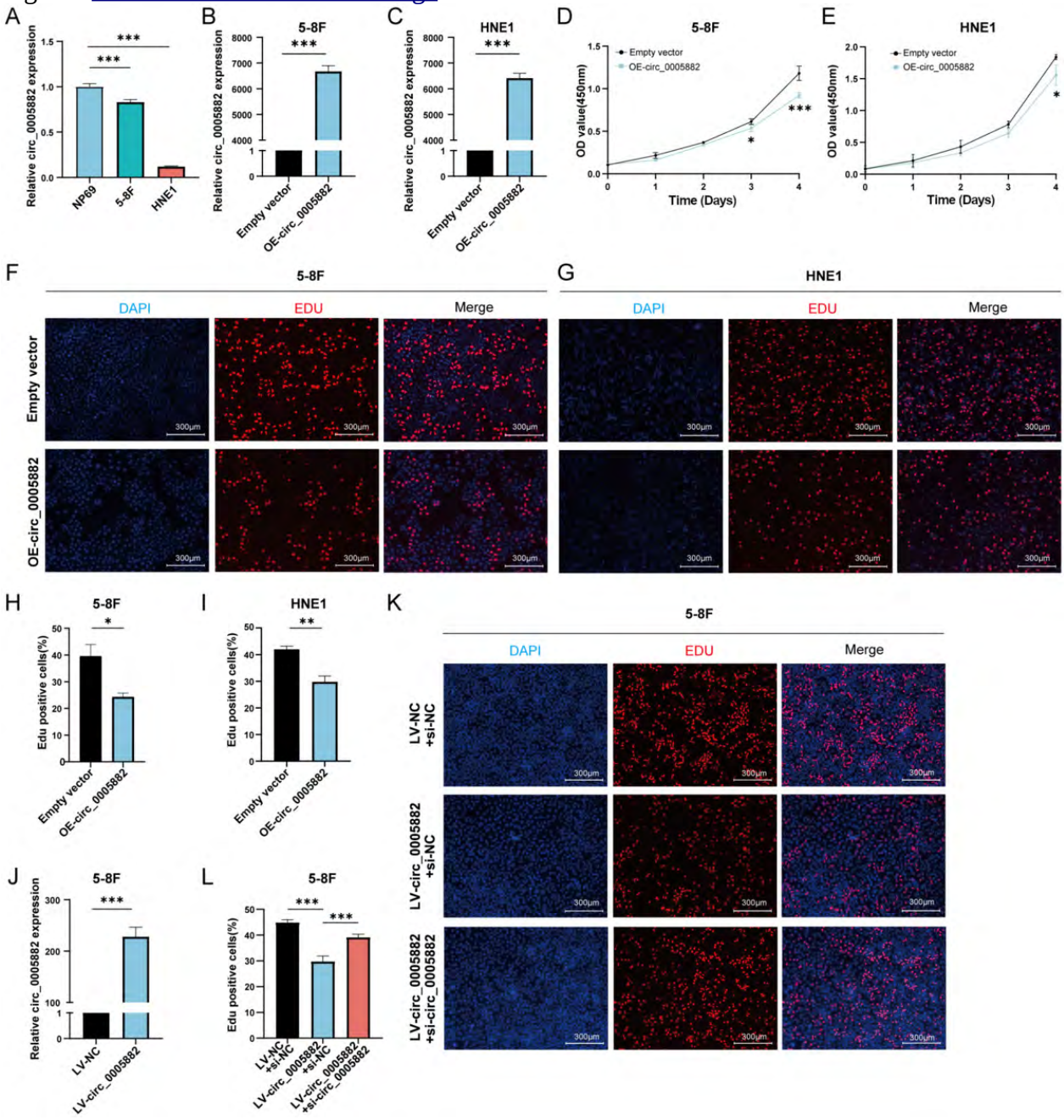

Fig. 3 [Download full resolution image]

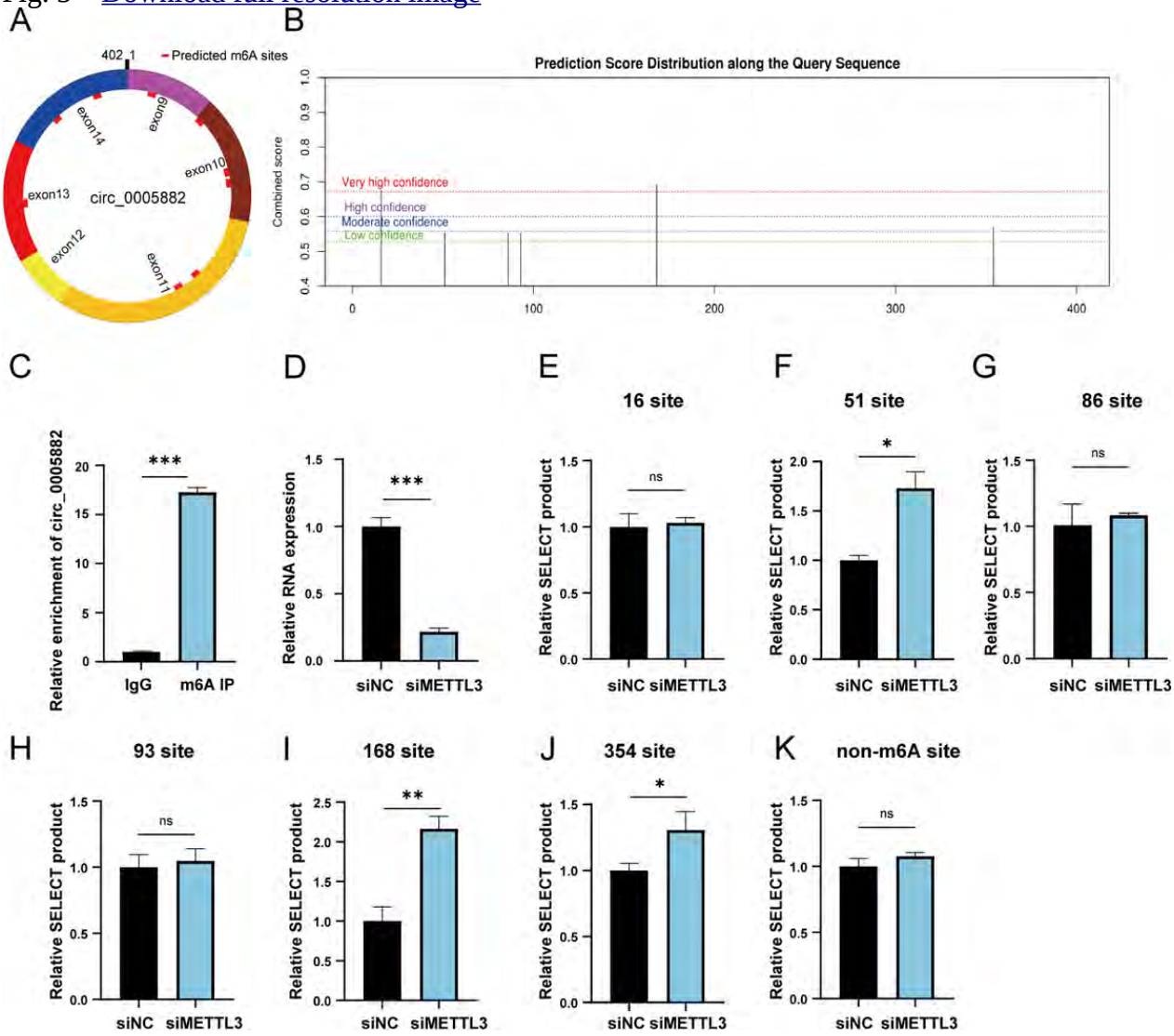

Fig. 4 [Download full resolution image]

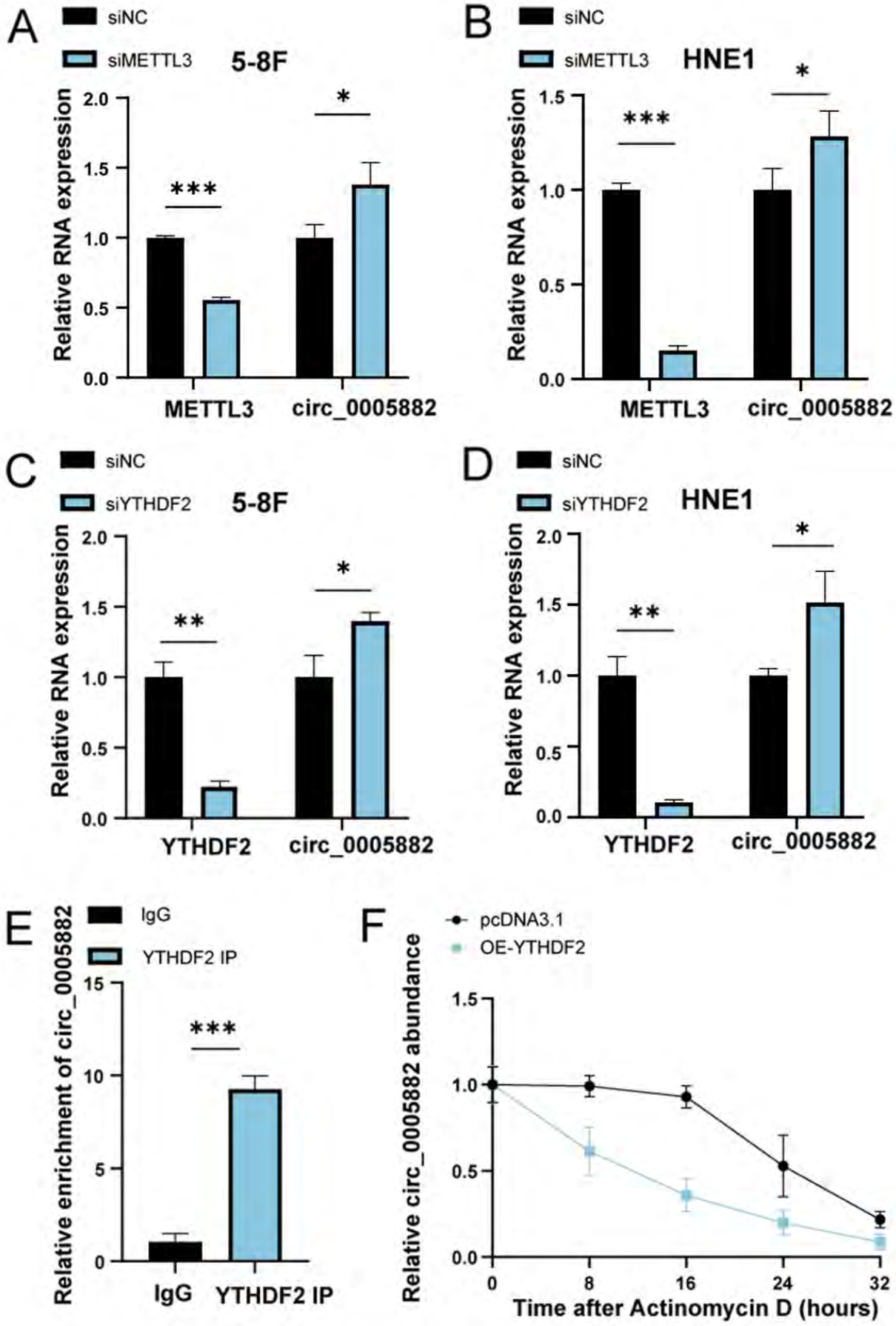

Fig. 5 Download full resolution image

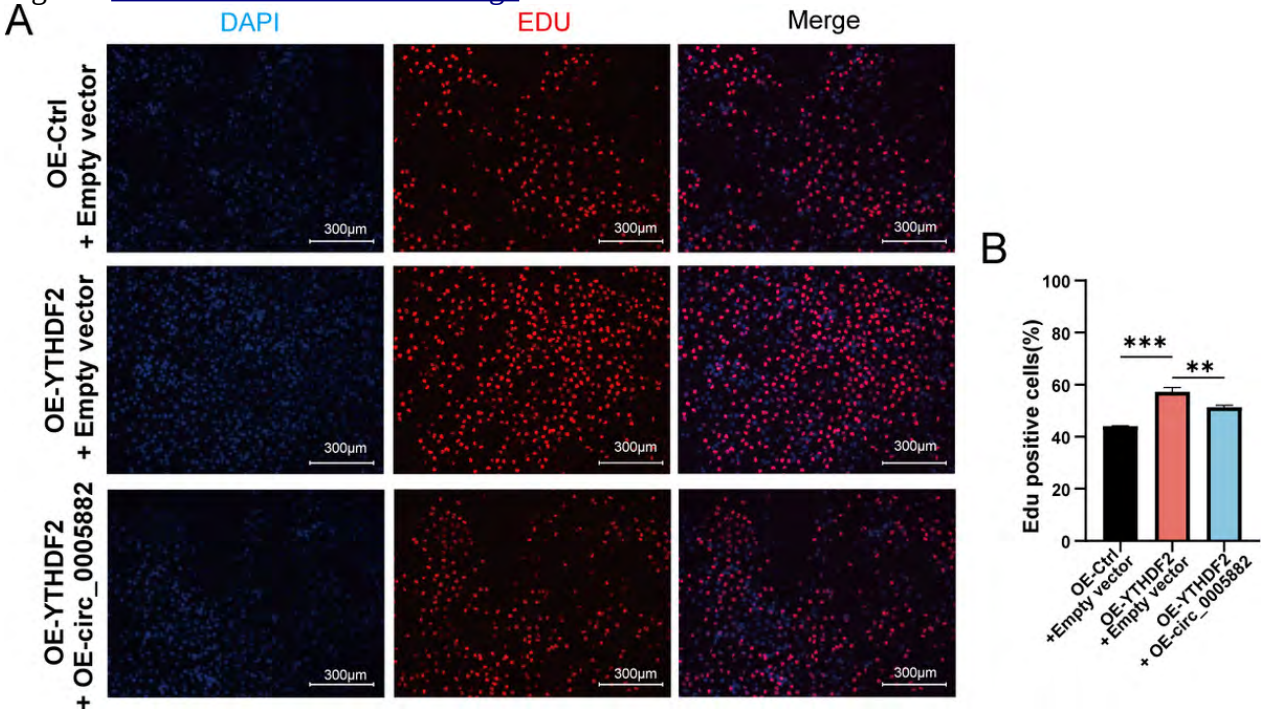

Fig. 6 [Download full resolution image]

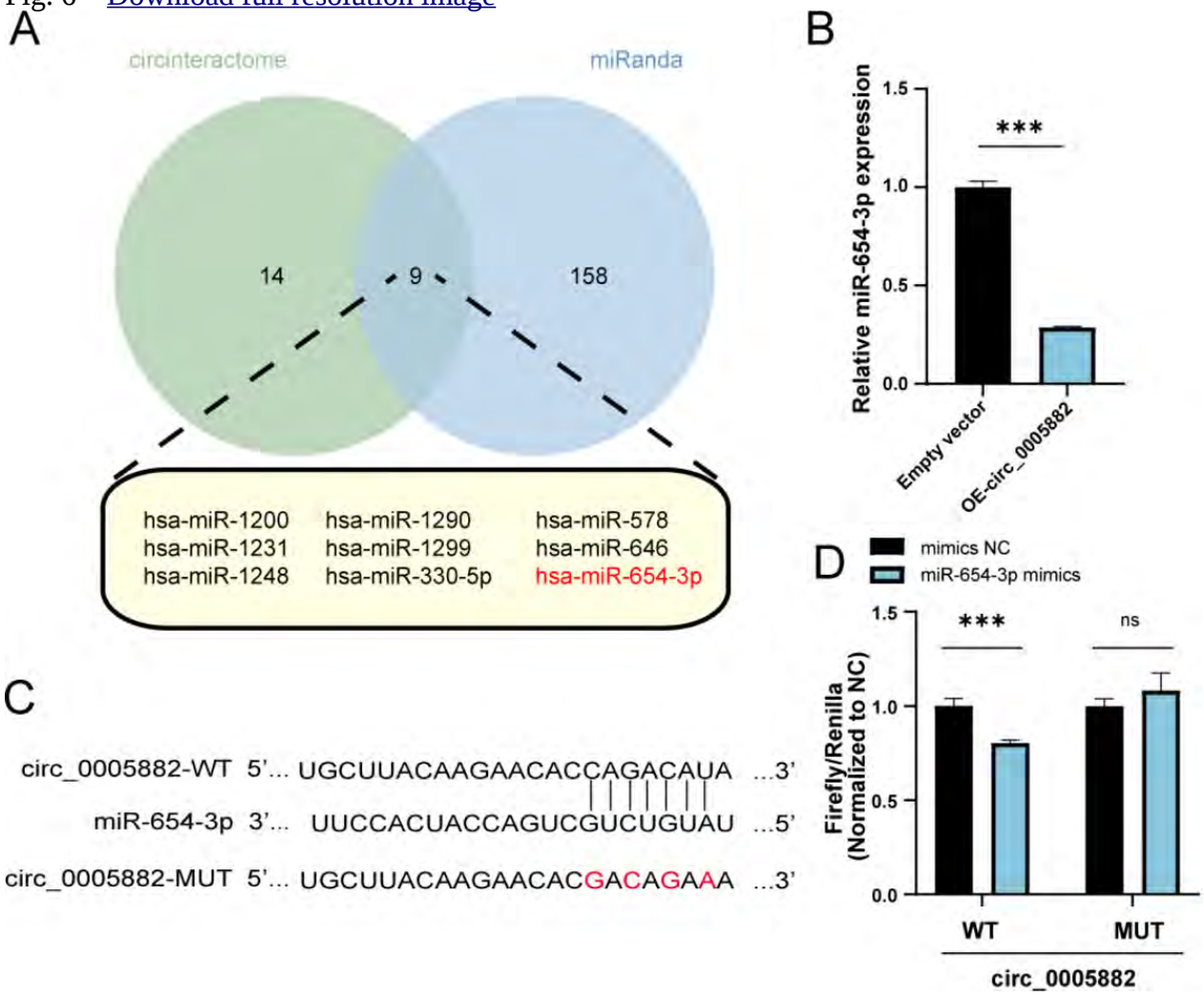

Fig. 7 Download full resolution image

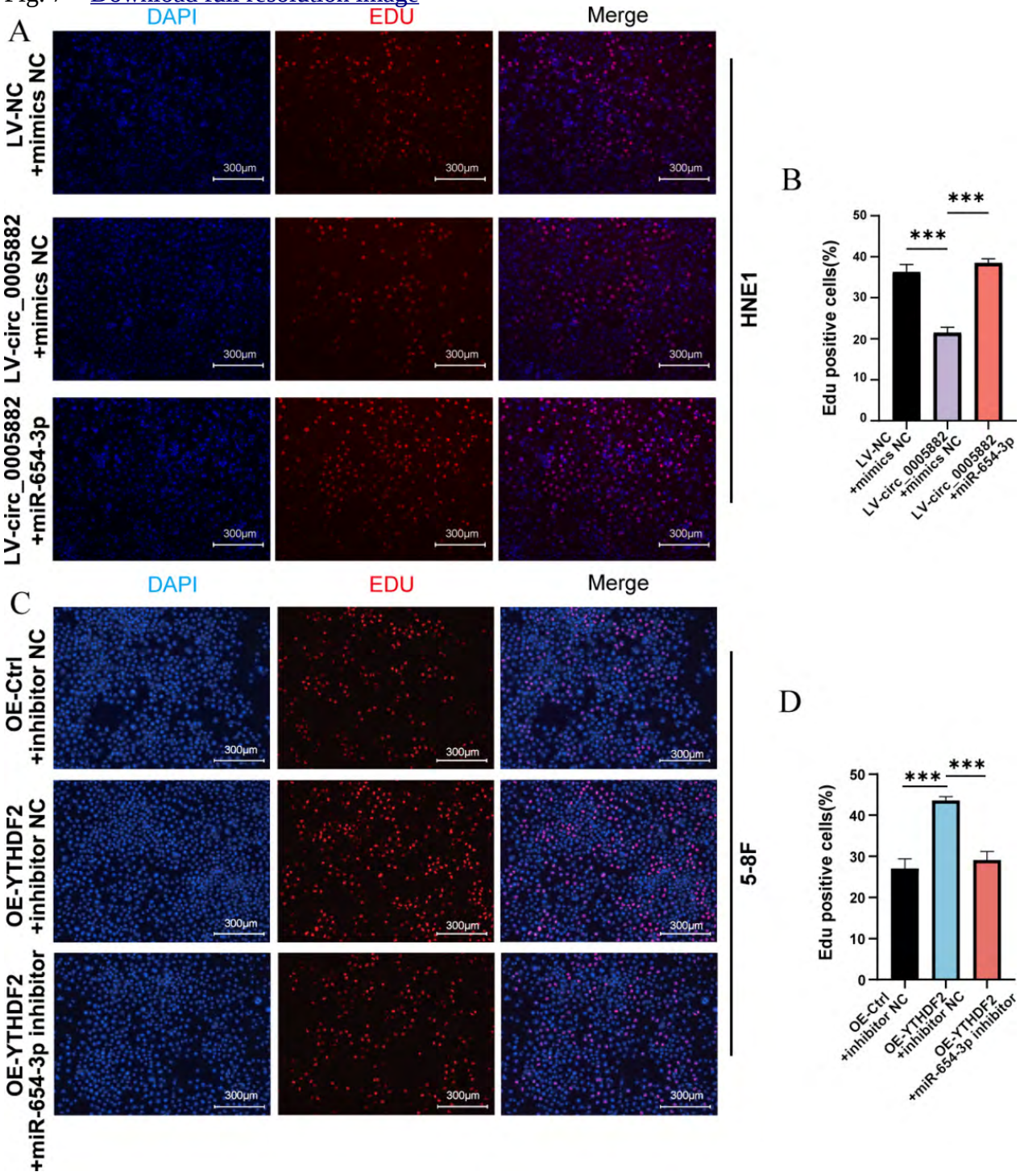

Fig. 8 Download full resolution image